

Aqueous Transformations of Zincophosphate Microporous Materials: Influence of Framework Topology

Ramsharan Singh, John Doolittle, Jr., and Prabir K. Dutta*

Department of Chemistry, The Ohio State University, 120 W. 18th Avenue, Columbus, Ohio 43210

Received: April 26, 2001; In Final Form: December 18, 2001

This paper reports on the acid-promoted dissolution of microporous zincophosphate frameworks of faujasite (ZnPO-X) and sodalite (ZnPO-S) topologies. Elemental analysis of the solution as well as local pH changes around the dissolving crystallites were measured. In addition, diffraction and electron microscopy of the resulting solid that formed on the microporous zincophosphates upon dissolution was examined. It was found that hopeite, $\text{Zn}_3(\text{PO}_4)_2$, was formed in both cases, though with quite distinct sizes, being of the order of $\sim 1 \mu\text{m}$ on ZnPO-X and $\sim 30 \mu\text{m}$ on ZnPO-S. The hopeite coating on ZnPO-X was dense as compared to that on ZnPO-S. The local pH change around the dissolving crystal correlated well with hopeite formation. Both elemental analysis and pH measurements indicated that the formation of hopeite was more pronounced on the ZnPO-X. Upon gentle stirring of the medium around the dissolving crystallites, the pH changes around ZnPO-X and ZnPO-S became similar, suggesting similar hopeite formation rates. On the basis of these results, we propose that the nucleation of hopeite occurs on the zincophosphate surface via heterogeneous nucleation, with the nuclei coming from the dissolution products of ZnPO-X and ZnPO-S. Differences in the morphology of the hopeite are ascribed to the differences in dissolution products between ZnPO-X and ZnPO-S. The stronger perturbation of the stirring experiments on hopeite formation from ZnPO-X is interpreted as arising from the smaller size of the dissolution units and, hence, more susceptible to convection effects.

Introduction

Microporous solids form an important class of materials, characterized by porosity in the range of 2–15 Å. Of particular interest among this class of materials are aluminosilicate zeolites, which are extensively used in chemical, petrochemical, environmental, and consumer industries.¹ Besides Si and Al, elements such as Zn, P, Ga, and a host of other transition metals can also be a part of the microporous framework.² The framework elements are typically bonded to four oxygen atoms in a tetrahedral geometry. Such materials are typically synthesized using hydrothermal methods, in which the reactants go through a complex sequence of polymerization and depolymerization reactions to form nuclei that grow into crystals.³ Considerable research is presently focused on determining the factors that lead to the development of microporosity in the crystals. Over the past two decades, spectroscopic and scattering methods have focused on the earliest stages of crystal growth.^{4,5} Crystal growth has been proposed to occur by agglomeration of nanometer-sized nuclei into specific geometries which then superassemble to the crystal or by incorporation of the small nanometer units onto a growing crystal.^{6,7} How microporosity is generated during such crystal growth processes is not clear. It has been proposed that in the presence of organic molecules the organic–inorganic–water interactions are modified by electrostatic and hydrophobic forces to generate cavities, around which the inorganic structure links itself.⁸

Crystal dissolution has not been as extensively studied as crystal growth, though understanding the dissolution of the frameworks is also necessary for various reasons. Large pore microporous materials are metastable structures and dissolve

to be replaced by more condensed structures.³ Besides, crystal dissolution is of relevance in altering framework composition; that is, aluminosilicate zeolites are converted to more siliceous frameworks by a partial dissolution mechanism.⁹ Subotic and co-workers have made some of the most detailed analysis of dissolution of zeolites, including development of kinetic models, based on the rates of appearance of soluble silicate and aluminate species in solution.¹⁰ On a molecular level, very little work has been done on dissolution. Recently, an AFM study focused on dissolution of the zeolitic mineral heulandite and concluded that layers of aluminosilicates were removed from the dissolving crystal surface.¹¹

In this paper, we focus on dissolution of microporous frameworks made up of zinc and phosphorus atoms and are referred to as zincophosphates (ZnPO).¹² In particular, we compare and contrast the dissolution of zincophosphates with the faujasite (ZnPO-X) and sodalite topologies (ZnPO-S). The advantages of studying zincophosphates are 2-fold. ZnPO-S and ZnPO-X both have the same framework composition with $\text{Zn/P} = 1$, and the dissolution can be examined under ambient conditions. We report here that, under acidic conditions, both ZnPO-X and ZnPO-S dissolved with formation of a film of hopeite, $\text{Zn}_3(\text{PO}_4)_2$, on the dissolving crystals. The size distribution and particle morphology of the hopeite were distinct on ZnPO-X and ZnPO-S. Elemental analysis of the solution showed that the rate of appearance of the dissolved Zn and P was different for ZnPO-X and ZnPO-S. Use of a colorimetric acid–base indicator dye coupled with electronic spectroscopy provided a convenient probe for monitoring the pH around the dissolving crystals as a function of time. Perturbation of the dissolution via convective currents was examined. Overall, this study concludes that zincophosphates with different structures dissolve

* To whom correspondence should be addressed.

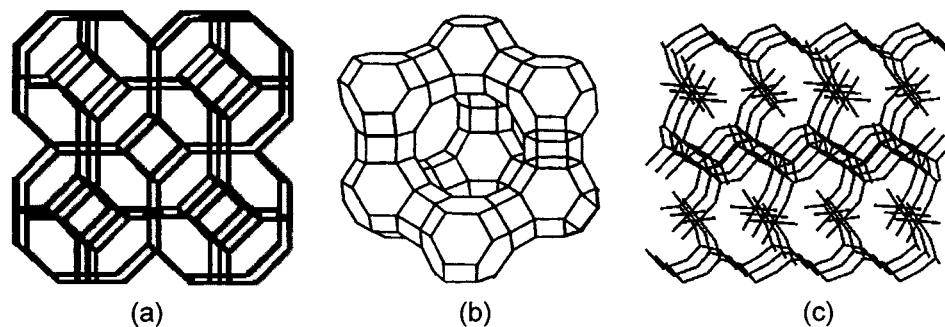


Figure 1. Framework structures of (a) ZnPO-S, (b) ZnPO-X, and (c) hopeite. In Figure 1a,b, the Zn–O–P bond is represented as a line, whereas in Figure 1c, the Zn–O–P bonds are explicitly shown.

by formation of distinct subunits, which leads to the different growth dynamics and, hence, morphologies of hopeite.

Thin films of hopeite are technologically relevant as coatings on steel for corrosion prevention,^{13a} exhibit high breakdown voltages,^{13b} and find use in electric motors and transformers and are present in dental ceramics.^{13c}

Experimental Section

Materials. Zinc nitrate hexahydrate (Aldrich, 98%), H_3PO_4 (AR Grade, Mallinckrodt, 85%), 1,4-diazabicyclo[2,2,2]octane (DABCO; Aldrich, 98%), tetramethylammonium hydroxide (TMAOH; 25% w/w, Sachem), and sodium hydroxide pellets (NaOH; 98.8%, Baker Analyzed) were used as received. Zincophosphates of framework type ZnPO-S and ZnPO-X were synthesized by following literature procedures.¹²

General Procedures. A citrate buffer solution of pH 3 was prepared by dissolving citric acid monohydrate, sodium hydroxide, and sodium chloride of concentrations 0.04, 0.021, and 0.06 M, respectively. Pellets of the zincophosphate materials were pressed by applying a pressure of $1.7 \times 10^4 \text{ N m}^{-2}$. Electronic spectroscopic analysis was carried out using a Shimadzu UV-265 spectrophotometer. The morphology of the crystallites of materials was characterized by SEM using a JEOL JSM-820 electron microprobe. Prior to examination, the samples were mounted with double-sided carbon paste tape on aluminum pegs and coated with a film of evaporated gold. Quantitative analysis of phosphorus and zinc ions in the water phase was carried out using a Perkin-Elmer Optima 3000 DV inductively coupled plasma optical emission spectrometer (ICP–OES). The X-ray powder patterns were determined with a Rigaku, D-Max-2B X-ray diffractometer using nickel filtered $\text{Cu K}\alpha$ ($\lambda = 1.5405 \text{ \AA}$) radiation.

Dissolution Experiments. Unstirred System. In a typical experiment, a sample of 0.0300 g of powder material was used to press a pellet of diameter size 8 mm. The pellet was placed carefully at the bottom of a spectrophotometric cell and 3 mL of the buffer solution (pH = 3) mixed with bromocresol green dye (dye concentration $\approx 1.6 \times 10^{-5} \text{ M}$ in buffer) was added slowly with a pipet, and the cell was immediately placed in the cell holder which was previously adjusted using aluminum spacers so that the light beam passes very close to the upper surface of the pellet (within 1 mm). UV–vis spectra were recorded at an interval of 15 min.

Stirred System. The stirring of the solution in the cell concurrently with the UV–vis spectral recording was achieved by using a motorized mechanical stirrer. This stirrer was designed to immerse through the top of the UV–vis cuvette, and the stirring range was controlled between 0 and 620 rpm. A Teflon crossbar was attached to the end of the stirring bar to

allow for a smooth stirring. The head of the crossbar was about 2 cm above the pellet.

ICP–OES Elemental Analysis. A sample of 0.2000 g of materials was used to press a pellet of diameter size 13 mm. The pellets were placed in screw capped glass vials, and 10 mL buffer solution of pH = 3 was added carefully to each vial, and the vials were closed. The solution was carefully drained using a 25 mL pipet at the desired time interval. These solutions were analyzed for Zn and P concentration using ICP–OES spectroscopy.

Results

Figure 1 shows the structures of the two frameworks, ZnPO-X and ZnPO-S, whose dissolution has been examined in this study, as well as a condensed zincophosphate, hopeite. All experiments were carried out with pressed pellets of ZnPO-S and ZnPO-X crystallites in a buffer of pH ~ 3 . The pressed pellets made it convenient to examine both solution and solid phases. The dissolution of ZnPO-X made with two structure directing agents, DABCO and TMAOH, were studied. The consequences of dissolution, as determined by a variety of methods, were found to be very similar for ZnPO-X made with DABCO or TMAOH; thus, the results presented in this paper deal with the TMA-derived crystals.

Crystal Dissolution in an Unstirred Environment. a. Powder Diffraction. Figure 2a,b show the powder diffraction data obtained from the top surface of the pellets of ZnPO-S and ZnPO-X before and after exposure to the pH ~ 3 buffer. In both samples, the peaks from the parent crystals decreased with time and there was the appearance of a new set of peaks. These new reflections were readily assigned to $\text{Zn}_3(\text{PO}_4)_2$, commonly known as hopeite.¹⁴ The peaks that were due to hopeite obscured those from the underlying ZnPO-X much more rapidly (within the first hour) than they did with ZnPO-S, where the signal that was due to the parent crystal was observed even after 4 h.

b. Electron Microscopy. Figure 3 compares the SEM micrographs of the starting ZnPO-S and ZnPO-X powders used in this study. The ZnPO-X crystals were octahedral and reasonably uniformly sized of about $5 \mu\text{m}$, whereas the ZnPO-S crystals were not as well defined and slightly smaller, yet single-crystal units and not agglomerates. Figure 4a,b shows the surfaces of the ZnPO-S and ZnPO-X pellets, respectively, after exposure times of 1 and 4 h to pH 3 buffer. It was clear that, upon exposure to acid, a new layer was forming on the original crystal. Because this surface has the diffraction pattern characteristic of hopeite (Figure 2), the composition of the new layer is $\text{Zn}_3(\text{PO}_4)_2$. However, the crystal morphology of hopeite was quite distinct on ZnPO-S and ZnPO-X, with much larger crystals on ZnPO-S ($\sim 30 \mu\text{m}$) than on ZnPO-X ($\sim 1 \mu\text{m}$). For ZnPO-S,

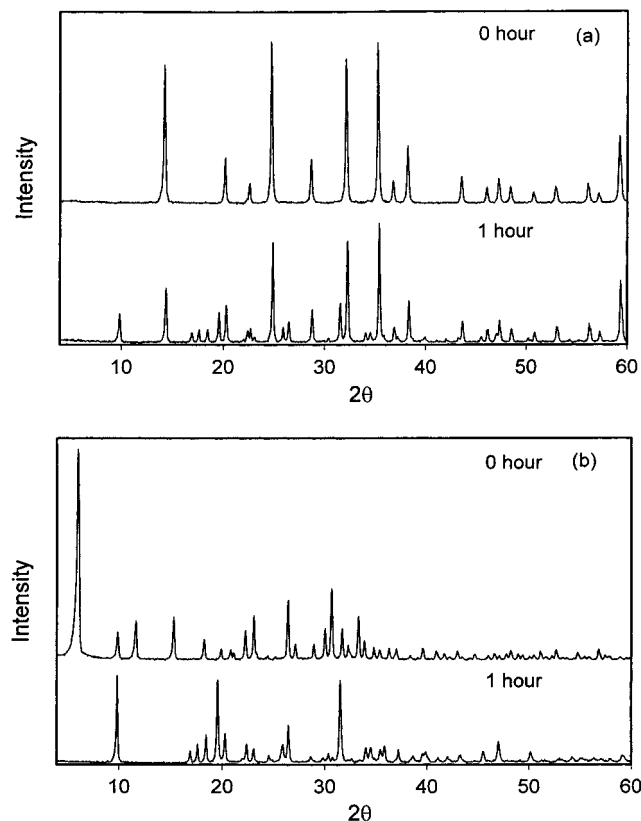


Figure 2. Powder diffraction patterns of pellets of (a) ZnPO-S and (b) ZnPO-X after 0 and 1 h of exposure to pH \sim 3 buffer.

the sodalite crystals can be seen clearly between the hopeite crystals on the surface. The side view of the ZnPO-X pellet (Figure 5) after 2 h of exposure shows that the bottom of the pellet is still ZnPO-X and that hopeite forms a pretty dense layer of 200 μm on the top of the pellet.

c. Elemental Analysis of the Solution Phase during Crystal Dissolution. The solution phase was analyzed for both Zn and P by ICP-OES during crystal dissolution and the data are presented in Figure 6. Even though the composition of both frameworks was Zn/P = 1, the elemental analysis showed that the solution became considerably more enriched in P than in Zn. During the time period of 2–5 h, there appeared to be a fairly linear relationship for the appearance of Zn and P in solution. The difference to note between ZnPO-X and ZnPO-S was that the appearance of P in solution was comparable for both, whereas the amount of zinc and the rate of its release (by a factor of 2) was smaller for ZnPO-X.

d. pH Changes during Crystal Dissolution. Change in pH can be readily measured by monitoring the absorption or fluorescence spectra of dye molecules in solution. Using bromocresol green as an indicator, we measured the transient change in pH above a ZnPO-X and ZnPO-S pellet buffered at pH \sim 3. From a titration of bromocresol green as a function of pH, a calibration curve based on the intensities of the acidic ($\lambda_{\text{max}} \sim 441 \text{ nm}$) and basic ($\lambda_{\text{max}} \sim 615 \text{ nm}$) forms of the indicator was established. When a pellet of zincophosphate was introduced into a pH \sim 3 buffer containing bromocresol green, it was noted that the yellow color of the dye solution just above the settled pellet (about a length of 1 cm) turned to a greenish color, indicating an increase in pH above the dissolving crystallites. The absorption spectrum of the dye was monitored in this region above the pellet (about 1 mm above the pellets) as a function of time and is shown in Figure 7. The system was left completely undisturbed during the measurements.

From the absorption spectra in Figure 7 and the pH calibration curve, the pH changes around ZnPO-X and ZnPO-S were determined and the data plotted in Figure 8a. The pH change around the ZnPO-X was more marked than around ZnPO-S, and in both cases, the solution around the dissolving crystal was becoming more basic. The measurement at time zero coincided with adding the buffer to the pellet, and the baselines were not yet established. The data were considered from a time of 15 min.

Crystal Dissolution in a Stirred Environment. Another series of experiments were done with gentle stirring of the medium with a stirrer positioned from the top of the cell, and extending to about 2 cm above the pellet (details in the Experimental Section). Stirring speeds up to 600 rpm were studied. As long as the stirring speeds were kept below 100 rpm, it was possible to keep the colored plume above the dissolving crystal with a similar appearance to the unstirred samples. At higher speeds, eventually the whole solution turned bluish-green because the stirring was intense enough to promote considerable dissolution of the pellet and overwhelming of the buffer. Figure 8b shows the comparison of the pH changes above the dissolving crystals for stirring speeds of 100 rpm. At the higher stirring speeds of 100 rpm, there was a decrease in the absolute magnitude of the pH gradient, because of the stirring. More importantly, as the stirring speed increased, the pH changes around the dissolving ZnPO-X and ZnPO-S appeared to be merging. Increased convection should lead to enhanced dissolution because the concentration of the zinc and phosphate species at the surface of the dissolving ZnPO decreases. The SEM micrographs of the ZnPO-X and ZnPO-S pellets after 4 h at the 100 rpm stirring are shown in Figure 9.

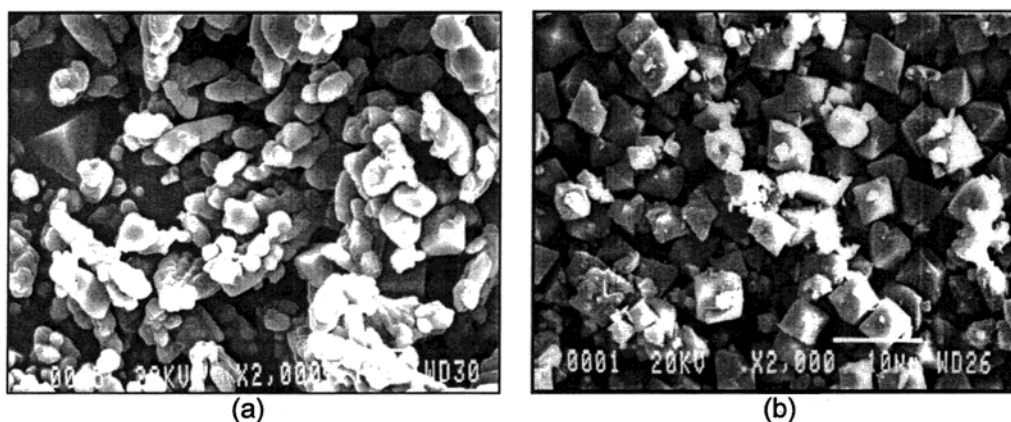


Figure 3. SEM micrographs of powders of (a) ZnPO-S and (b) ZnPO-X.

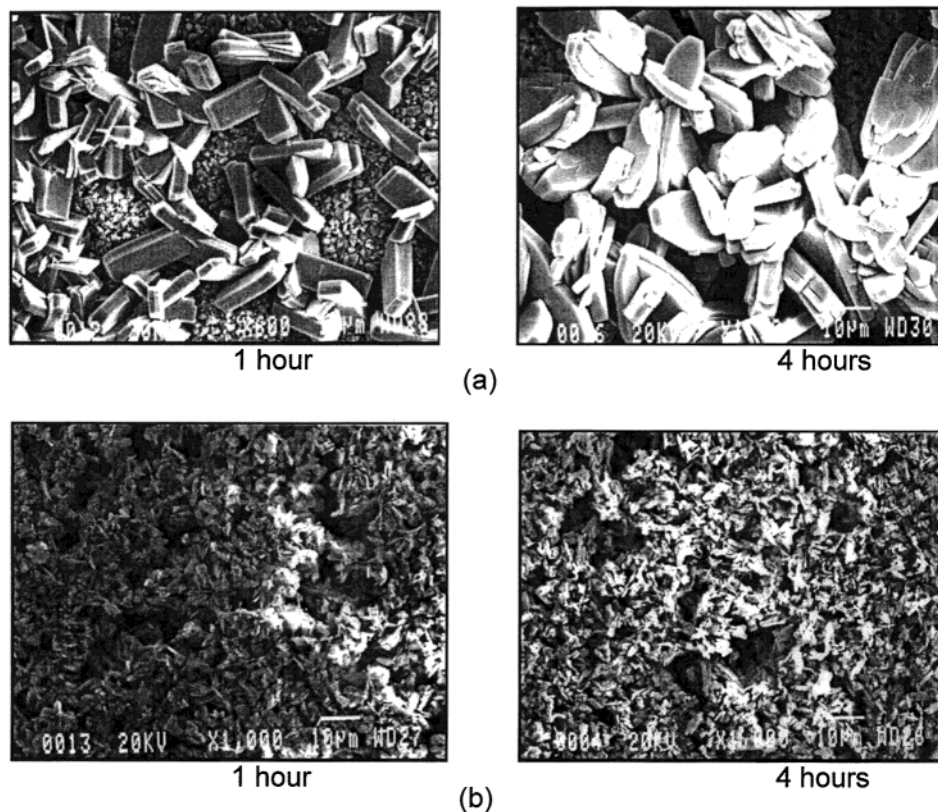


Figure 4. SEM micrographs of pellets of (a) ZnPO-S and (b) ZnPO-X after 1 and 4 h of exposure to pH \sim 3 buffer (unstirred system).

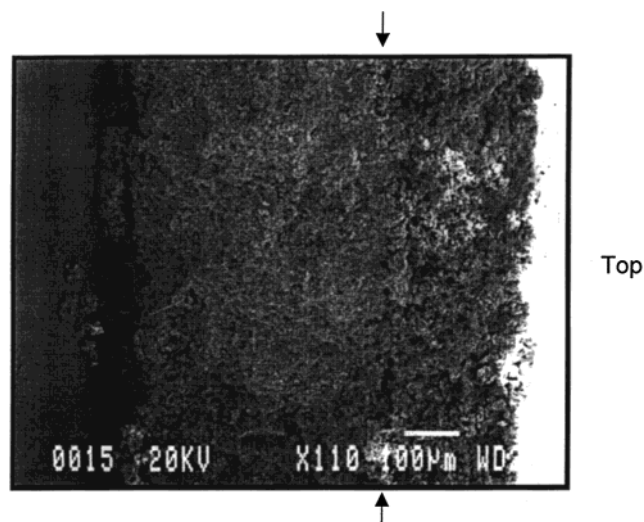


Figure 5. SEM micrograph of a side view of ZnPO-X after 2 h exposure to pH \sim 3 buffer (unstirred system). The layer to the right of the arrows is hopeite.

Discussion

Hopeite Formation. *a. Unstirred System.* The powder diffraction data (Figure 2) clearly indicates that in both ZnPO-X and ZnPO-S dissolution, hopeite is being formed as the product at pH \sim 3. Electron microscopy shows that the morphology of the hopeite formed in both cases is quite distinct. In ZnPO-X, the hopeite crystals are considerably smaller and form a dense coating on the surface of the ZnPO-X pellet. For ZnPO-S, the hopeite crystals are considerably larger and do not completely cover the pellet surface. These differences in the hopeite microstructure explain the powder diffraction data in the case of ZnPO-X dissolution, where peaks only due to hopeite are observed after the first hour of reaction.

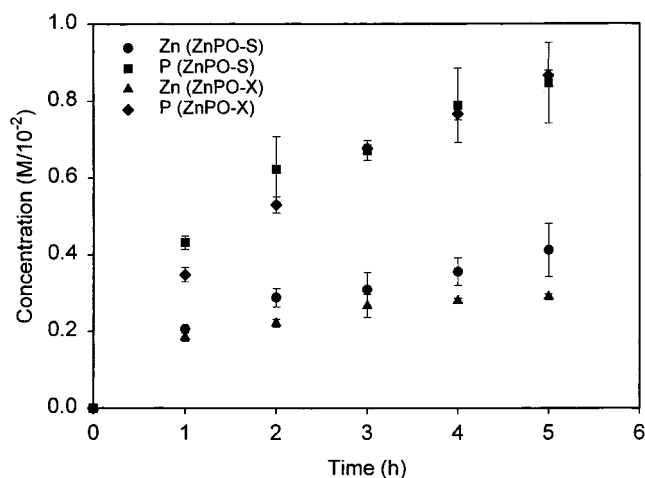
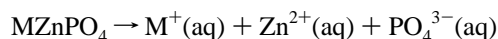


Figure 6. Elemental analysis of solutions of pellets of ZnPO-X and ZnPO-S exposed to pH \sim 3 buffer. Symbols represent ZnPO-S, Zn (●) and P (■), and ZnPO-X, Zn (▲) and P (◆). Concentrations were calculated based on a volume of \sim 10 mL of buffer.

Elemental analysis of the solution shows the presence of both zinc and phosphorus. Thus, the dissolution chemistry must involve



Besides free zinc and phosphate ions, species such as $\text{ZnH}_2\text{PO}_4^+$ can also exist as ion-pairs.^{14cf} Hopeite crystals are made up of distorted ZnO_6 octahedra, ZnO_4 tetrahedra, and PO_4 tetrahedra units and four water molecules (Figure 1c).^{14g} Because the ZnPO frameworks contain only tetrahedral units, considerable structural rearrangement is required and a solid-state transformation is unexpected. Formation of hopeite occurs by

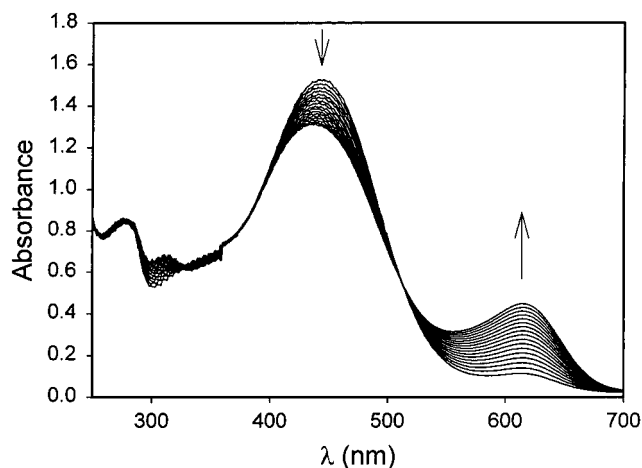


Figure 7. Absorption spectra of the solution above a dissolving ZnPO-S pellet as a function of time (spectra taken every 15 min) in a solution containing bromocresol green buffered at pH ~ 3 (unstirred system).

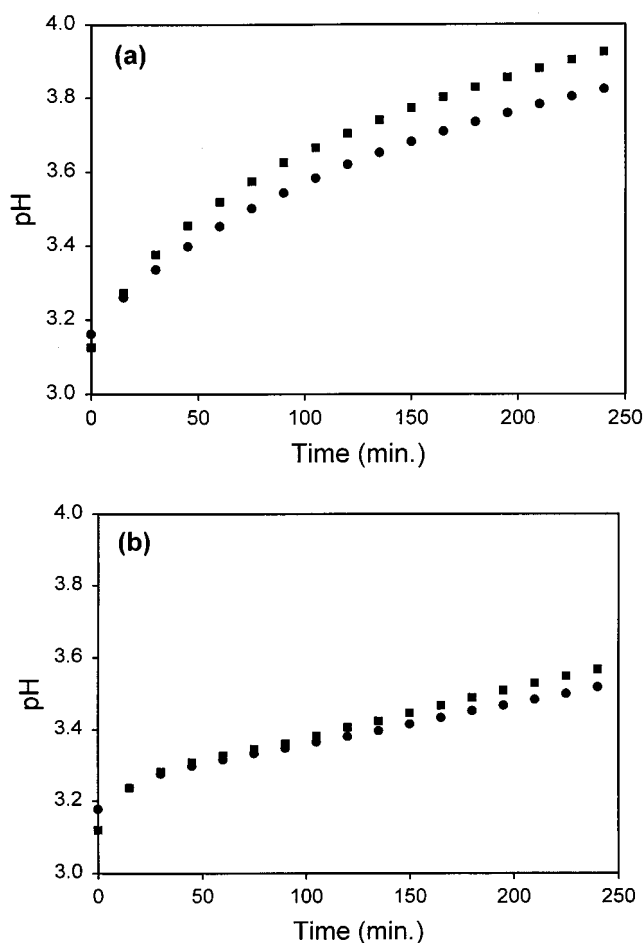
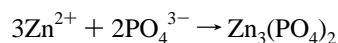


Figure 8. pH changes around dissolving ZnPO-S (●) and ZnPO-X (■) as a function of time for an (a) unstirred solution and (b) a solution stirred at 100 rpm.

the following reaction:



As the zincophosphate dissolves, supersaturation that initiates the nucleation of hopeite occurs around the pellet surface. The formation of hopeite is promoted because of its low solubility, K_{sp} being reported on the order of 10^{-35} .^{14c} The inequality in

the zinc and phosphorus concentrations in solution can then be attributed to the formation of hopeite. As hopeite crystals grow, the imbalance between the zinc and phosphate concentrations becomes marked in time. However, it is important to note that the divergence in the P and Zn concentration in time is more marked with ZnPO-X than ZnPO-S, though the overall moles of zinc and phosphorus in solution are comparable for both crystals. Thus, for ZnPO-X dissolution, the greater divergence of the phosphorus and zinc curves indicates that more of the dissolving nutrients from the crystal are incorporated in hopeite. This conclusion is consistent with the diffraction and electron microscopy data, which indicate more extensive nucleation of hopeite on the ZnPO-X surface. However, because hopeite also dissolves, the elemental analysis cannot be used quantitatively for estimating ZnPO dissolution or hopeite formation.

The colorimetric method provides a better estimate for hopeite formation. We have examined the dissolution of hopeite and find no change in pH around the dissolving crystal. This indicates that the hydrolysis of Zn^{2+} balances the pH increase from the phosphate. The dissolution of the framework zincophosphate structures with Zn/P = 1, to form hopeite, leads to the imbalance of Zn and phosphate that leads to the pH change. The increase in pH around the dissolving crystal can be readily explained as arising from reaction of PO_4^{3-} with H^+ to form $\text{HPO}_4^{2-}/\text{H}_2\text{PO}_4^-$. Thus, any changes in pH that we observe during ZnPO dissolution can be related to the formation of hopeite. The larger change in pH for the ZnPO-X system is consistent with the elemental analysis data and supports the model that hopeite growth is more pronounced on ZnPO-X as compared to the ZnPO-S system.

b. Stirred System. The noninvasive nature of the spectroscopic measurement made it possible to study the pH change with gentle stirring. Previous studies of CaCO_3 precipitation have shown marked changes in both the crystal habit and morphology upon stirring.¹⁵ The convection currents generated by stirring have several effects. They increase the dissolution of both ZnPO-X and ZnPO-S and, as evidenced from the diffraction data and SEM, result in formation of more hopeite. Stirring also increases the hopeite dissolution as evident from the SEM of the hopeite crystals for stirred and unstirred experiments. For the stirred samples, the hopeite crystals have a hollow groove in the slab-like crystals. Stirring has not changed the overall morphology of the hopeite crystals. The absolute change of pH diminishes with stirring, which is expected, because stirring reduces the H^+ concentration gradient established around the dissolving crystals. However, for a fixed stirring speed, the difference in pH between the ZnPO-X and ZnPO-S dissolution is a reflection of the dynamics of hopeite formation. Thus, with increasing stirring speeds, merging of the pH change between ZnPO-X and ZnPO-S reflect the fact that the rate of hopeite formation in both framework dissolutions are becoming similar.

Dissolution Mechanism. Perez and Nancollas have studied the growth of hopeite and concluded that the crystallization rate is controlled by factors such as incorporation of growth units at dislocations in the crystal surface or by the replacement of water molecules between the cation hydration layer and the solvent. The exact nature of the growth units was not determined.¹⁶

Previous studies on dissolution of microporous aluminosilicate materials provide some perspective about the dissolution mechanisms. Cizmek et al. have studied the dissolution of high-silica pentasil zeolites in caustic solution and found that organic-free zeolite dissolved more rapidly because the OH^- could penetrate deep into the framework.^{10c} In the present case of ZnPO-X and

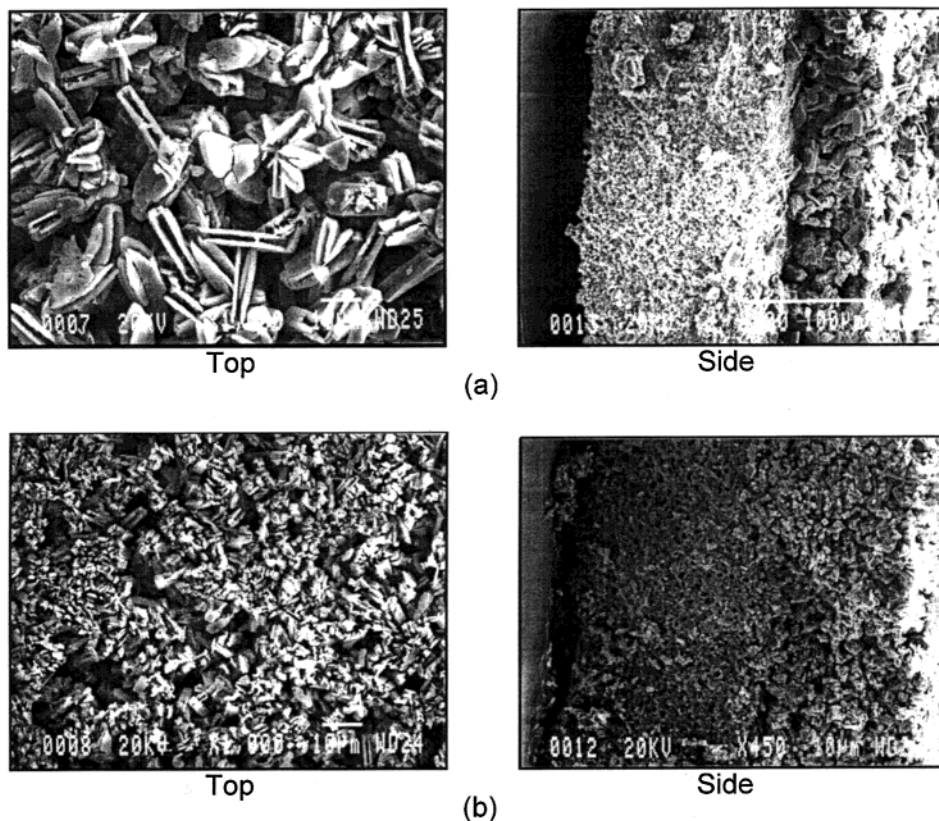


Figure 9. Top and side view SEM micrographs of pellets of (a) ZnPO-S and (b) ZnPO-X after 4 h of exposure to pH \sim 3 buffer, stirred at 100 rpm.

ZnPO-S dissolution, H^+ penetration with its hydration cell into the ZnPO-S framework is not expected, so dissolution is expected to occur from the surface. In the case of ZnPO-X, ion exchange of the Na^+ ions by H^+ can occur and dissolution can proceed from within the crystal.

Dissolution of zeolite A with Si/Al = 1 and, therefore, comparable to the present ZnPO with Zn/P = 1 has been studied and was found to be congruent and no new phases were formed. The silicon and aluminum species in solution were primarily monomeric.^{10a} However, if the zeolite A (K^+ -exchanged zeolite A) was made amorphous by thermal treatment and its dissolution examined, then zeolite A was found to form in solution, presumably because of the higher solubility of the amorphous material over the porous zeolite network.^{10d} This is surprising in view of the fact that the amorphous condensed material has to dissolve from the outer surface, whereas the zeolite allows for penetration of the solubilizing agents into the zeolite.

Dissolution of some zeolites can lead to the formation of secondary phases, such as amorphous SiO_2 from ZSM-5, and for different crystalline modifications of SiO_2 or different hydrates of sodium silicate upon dissolution of silicalite-1.^{10c} These secondary phases were thought to form by reaction of solubilized species in the solution or by reaction on the surface of the dissolving solid. Thus, the amorphous precipitate on the ZSM-5 surface was proposed to occur by reaction of silicate ions in solution with the ZSM-5 surface.

The simplest possibility for hopeite formation is that the frameworks are dissolving to form zinc and phosphate, which then exceed supersaturation to form hopeite. However, considering the differences in morphology and the dynamics of hopeite formation and that the overall levels of solubilized zinc and phosphate are comparable, as evident from the elemental analysis, we do not favor this mechanism.

A more likely possibility is that the hopeite is nucleated on or very close to the surface of the dissolving crystal from the intermediate dissolution products prior to the species escaping into the solution. This would be supported by an earlier paper, in which we examined the dissolution of a single crystal of ZnPO-X (rather than a large collection of crystals as in a pellet) and found that even slight convective motion around the dissolving crystal led to complete absence of hopeite.¹⁷ Thus, if the dissolving species are removed from the surface, hopeite can no longer be nucleated. The process of heterogeneous nucleation on the zincophosphates can occur at lower supersaturation and can be promoted by the surface structure.¹⁸ In this process, the number of crystals is a reflection of the number of heteronuclei, and so in the ZnPO-X dissolution, a larger number of heteronuclei are being formed.

The assumption that formation of precipitates, such as $Zn_3(PO_4)_2$, occur by simple stoichiometric reactions between Zn^{2+} and PO_4^{3-} may not be correct. For example, in the precipitation of Ag_2WO_4 from Ag^+ and WO_4^- , the presence of polymeric species $W_6O_{21}^{2-}$, $HW_6O_{21}^{5-}$, and $W_{12}O_{41}^{10-}$ needs to be considered.¹⁹ Similarly for $Fe(OH)_3$ precipitation, the experimental results are best explained by reaction of $Fe_9(OH)_{20}^{7+}$ and $Fe_3(OH)_4^{4+}$, rather than reaction between Fe^{3+} and $3 OH^-$.²⁰ We propose the hypothesis that the nuclei of hopeite arise from intermediate dissolution products of the zincophosphate frameworks. Because of the differences in the framework structure and the access of protons to the framework, the dissolution units are structurally different and result in the formation of hopeite of distinct morphologies. Small crystals are expected to grow faster than larger crystals for diffusion-controlled processes. The pH studies indicate that the hopeite formation on ZnPO-X is more pronounced than that on ZnPO-S and could be a reflection of the smaller crystals and diffusion-controlled growth.

Influence of convection on crystal growth has been studied.²¹ We propose that the convection currents generated by stirring influences the dissolution units arising from the two ZnPO surfaces differently. Convection currents can have two inter-related effects. First, by removing the dissolution products from the surface of the dissolving pellet, they promote further dissolution. Second, smaller dissolution units will be influenced to a larger extent by convection than the bigger units. In the unstirred system, the pH change, a measure of the hopeite growth, is steeper for ZnPO-X than ZnPO-S. Upon stirring, the overall dissolution of both frameworks increase, but the pH change, reflecting hopeite growth, merges. So, stirring has reduced the growth of hopeite on the ZnPO-X relative to ZnPO-S and is consistent with the ZnPO-X giving rise to smaller dissolution units and more susceptible to stirring. Differences in the dissolution units between ZnPO-X and ZnPO-S at the molecular level arise because of differences in their framework structure.

Conclusions

Dissolution of two microporous frameworks with faujasite (ZnPO-X) and sodalite (ZnPO-S) topologies has been examined. Elemental analysis of the solution shows the presence of both zinc and phosphorus, whereas diffraction and electron microscopy confirm that $Zn_3(PO_4)_2$ (hopeite) is formed on the dissolving ZnPO-X and ZnPO-S. The morphology of the hopeite was quite distinct, $\sim 1 \mu\text{m}$ crystallites on ZnPO-X and $\sim 30 \mu\text{m}$ on ZnPO-S. The hopeite growth on ZnPO-X leads to a dense film, whereas on ZnPO-S, a collection of large crystallites were observed. Local pH changes around the dissolving ZnPO-X and ZnPO-S were measured, and the solution was found to become more basic in both cases but more so around the ZnPO-X. The increase in basicity was correlated with formation of hopeite from zincophosphates with framework Zn/P = 1, leading to excess phosphate ions in solution. Both the elemental analysis and pH studies suggested that hopeite formation was more pronounced on the ZnPO-X surface. Mild convection currents generated by stirring led to equalization of the pH changes for both ZnPO-X and ZnPO-S dissolution. The data were explained on the basis of the hypothesis that hopeite was formed on the zincophosphate via heterogeneous nucleation, with the nuclei being intermediate dissolution products (rather than Zn^{2+} and phosphate ions) of the framework. The nucleation was more extensive on ZnPO-X, because the nuclei were smaller. This was also consistent with the effects of stirring, which led to increased loss of the nuclei because of their size for ZnPO-X as compared to ZnPO-S. Overall, this study provided evidence that the dissolution of microporous frameworks with different topologies proceeded via formation of distinct subunits, though no information on the structural features of these subunits were obtained. It is the formation of hopeite from both ZnPO-S and ZnPO-X that made this study possible.

Acknowledgment. We acknowledge funding from NASA for this research. Helpful discussions with Dr. Brian Schoeman from Dow Chemical and Dr. N. Ramachandran from NASA-Marshall are gratefully acknowledged. We would also like to thank Mr. John Sullivan for constructing the stirring apparatus.

References and Notes

- (1) *Proceedings of the 12th International Zeolite Conference*; Treacy, M. M. J., Marcus, B. K., Bisher, M. E., Higgins, J. B., Eds.; Materials Research Society: Warrendale, PA, 1999.
- (2) Szostak, R. *Handbook of Molecular Sieves*; Van Nostrand: New York, 1992.
- (3) Breck, D. W. *Zeolite Molecular Sieves*; John-Wiley: New York, 1974.
- (4) (a) Dutta, P. K. *J. Inclusion Phenom. Mol. Recognit. Chem.* **1995**, *21*, 215. (b) Kirschhock, C. E. A.; Ravishankar, R.; Verspeurt, F.; Grobet, P. J.; Jacobs, P. A.; Martens, J. A. *J. Phys. Chem.* **1999**, *103*, 4965–4971. (c) Gora, L.; Streleky, K.; Thompson, R. W.; Phillies, G. D. L. *Zeolites* **1997**, *18*, 119–131. (d) Anderson, M. W.; Agger, J. R.; Thornton, J. T.; Forsyth, N. *Angew. Chem., Int. Ed. Engl.* **1996**, *35*, 1210–1213.
- (5) (a) de Moor, P.-P. E. A.; Beelen, T. P. M.; van Santen, R. A. *J. Phys. Chem B* **1999**, *103*, 1639. (b) Watson, J. N.; Iton, L. E.; Keir, R. I.; Thomas, J. C.; Dowling, T. L.; White, J. W. *J. Phys. Chem. B* **1997**, *101*, 10094–10104.
- (6) (a) Schoeman, B. J. *Microporous Mater.* **1997**, *9*, 267–271. (b) Kirschhock, C. E. A.; Ravishankar, R.; Jacobs, P. A.; Martens, J. A. *J. Phys. Chem. B* **1999**, *103*, 11021–11027.
- (7) Nikolakis, V.; Kokkoli, E.; Tirrell, M.; Tsapatsis, M.; Vlachos, D. G. *Chem. Mater.* **2000**, *12*, 845–853.
- (8) Burkett, S. L.; Davis, M. E. *J. Phys. Chem.* **1994**, *98*, 4647–4653.
- (9) Bartl, P.; Holderich, W. F. *Microporous Mesoporous Mater.* **2000**, *38*, 279–286.
- (10) (a) Cizmek, A.; Komunjer, L.; Subotic, B.; Siroki, M.; Roncevic, S. *Zeolites* **1991**, *11*, 258–264. (b) Antonic, T.; Cizmek, A.; Kosanovic, C.; Subotic, B. *J. Chem. Soc., Faraday Trans.* **1993**, *89* (11), 1817–1822. (c) Cizmek, A.; Kosanovic, C.; Smit, I.; Tonejc, A.; Aiello, R.; Crea, F.; Nastro, A. *Microporous Mater.* **1997**, *8*, 159–169. (d) Kosanovic, C.; Subotic, B.; Kaucic, V.; Skreblin, M. *Phys. Chem. Chem. Phys.* **2000**, *2*, 3447–3451.
- (11) Yamamoto, S.; Sugiyama, S.; Matsuoko, O.; Kohmura, K.; Honda, T.; Banno, Y.; Nozoye, H. *J. Phys. Chem.* **1996**, *100*, 18474–18482.
- (12) (a) Nenoff, T. M.; Harrison, W. T. A.; Gier, T. E.; Stucky, G. D. *J. Am. Chem. Soc.* **1991**, *113*, 378. (b) Gier, T. E.; Harrison, W. T. A.; Nenoff, T. M.; Stucky, G. D. In *Molecular Sieves*; Ocelli, M. L., Robson, H., Eds.; Van Nostrand: New York, 1992, 407. (c) Reddy, K. S. N.; Salvati, L. M.; Dutta, P. K.; Abel, P. E.; Suh, K. L.; Ansari, R. R. *J. Phys. Chem.* **1996**, *100*, 9870. (d) Castagnola, M. J.; Dutta, P. K. *Micropor. Mater.* **2000**, *34*, 61. (e) Singh, R.; Dutta, P. K. *Langmuir* **2000**, *16*, 4148. (f) Singh, R.; Castagnola, M.; Dutta, P. K. *Reactions and Synthesis in Surfactant Systems*; Texter, J., Ed.; Marcel-Dekker: New York, 2001; p 737–760.
- (13) (a) Nair, U. B.; Subbaiyan, M. *J. Mater. Sci.* **1995**, *30*, 2108. (b) Weng, D.; Jokieli, P.; Uebles, A.; Boehni, H. *Surf. Coat. Technol.* **1996**, *88*, 147. (c) Margerit, J.; Cluzel, B.; Leloup, J. M.; Nurit, J.; Pauvert, B.; Terol, A. *J. Mater. Sci. -Mater. Med.* **1996**, *7*, 623.
- (14) (a) Umegaki, T.; Okabe, T.; Omori, K. *Bull. Chem. Soc. Jpn.* **1969**, *42*, 1304–1307. (b) Goloshchapov, M. V.; Filatova, T. N. *Russ. J. Inorg. Chem.* **1969**, *14* (3), 424–426. (c) Nriagu, J. *Geochim. Cosmochim. Acta* **1973**, *37*, 2357–2361. (d) Nikonenko, E. A.; Olikov, I. I.; Marenkova, I. N.; Margolin, L. N.; Reznikova, L. A. *Russ. J. Inorg. Chem.* **1985**, *30* (1), 13–16. (e) Margerit, J.; Cluzel, B.; Leloup, J. M.; Nurit, J.; Pauvert, B.; Terol, A. *J. Mater. Sci. - Mater. Med.* **1996**, *7*, 623–628. (f) Pawlig, O.; Trettin, R. *Mater. Res. Bull.* **1999**, *34* (12/13), 1959–1966. (g) Hill, R. J.; Jones, J. B. *Am. Mineral.* **1976**, *987*–995.
- (15) Ataka, M.; Fukushima, N.; Kitamura, M.; Ohtaki, H.; Okada, I.; Sato, K.; Sawada, K.; Shigematsu, K.; Ueno, S.; Waizumi, K. In *Crystallization Processes*; Ohtaki, H., Ed.; John Wiley & Sons: Chichester, U.K., 1998; Vol. 3.
- (16) Perez, L.; Nancollas, G. H. *J. Cryst. Growth* **1984**, *66*, 412–418.
- (17) Castagnola, M. J.; Dutta, P. K. *Microporous Mesoporous Mater.* **2001**, *42*, 235–243.
- (18) Garside, J.; Sohnle, O. *Precipitation: Basic Principles and Industrial Applications*; Butterworth-Heinemann: Oxford, U.K., 1992.
- (19) Jensen, J. B.; Lou, J. *Acta Chem. Scand.* **1983**, *A37*, 617–629.
- (20) van der Woude, J. H. A.; deBruyn, P. L. *Colloids Surf.* **1983**, *8*, 55–78.
- (21) Chen, P. S.; Shlichta, P. J.; Wilcox, W. R.; Lefever, R. A. *J. Cryst. Growth* **1979**, *47*, 43–60.